

## Study on the formation mechanism of algal floc driven by flow field in a helical tube flocculator

Chuanzhen Wang<sup>1</sup>, Yiming Zhang<sup>1,2</sup>, Xuezhi Zhang<sup>2</sup>, Haiyang Zhang<sup>1,2</sup>

<sup>1</sup> China Anhui Engineering Research Center for Coal Clean Processing and Carbon Reduction, College of Material Science and Engineering, Anhui University of Science and Technology, Huainan 232001

<sup>2</sup> Institute of Hydrobiology, Chinese Academy of Sciences, Wuhan, Hubei 430072, China

Corresponding author: [hyzhang@ihb.ac.cn](mailto:hyzhang@ihb.ac.cn) (Haiyang Zhang)

**Abstract:** The tubular flocculation reactor is a new device for the efficient treatment of algal wastewater, which has the characteristics of high removal efficiency and small dosage of chemicals. The mechanism of the influence of the flow field on the formation of floc in the pipeline has not been clarified. In this study, the effects of flow field distribution, reagent concentration and algal concentration on removal efficiency were investigated by means of experiment and numerical simulation. The results showed that the removal efficiency of the surface tubular flocculation reactor was related to the shape of the generated floc. When the size of the generated floc was greater than 900 $\mu\text{m}$  and the fractal dimension was greater than 1.25, the removal efficiency of the tubular flocculation reactor exceeded 90%, and the removal efficiency of the tubular flocculation reactor could eventually reach more than 98% with continued increase of the floc size and compactor degree. Under the same pipe diameter, the size and fractal dimension of flocs are linearly correlated with the proportion of inertial subregions in the flow field. After the flow rate is increased from 0.15m s<sup>-1</sup> to 0.3m s<sup>-1</sup>, the non-positive region of Q criterion in the pipeline is reduced by 3%, the size of flocs is reduced by 200 $\mu\text{m}$ , and the fractal dimension is decreased by 0.3.

**Keywords:** bloom treatment, tubular coagulation reactor, floc morphology, flow field distribution, numerical simulation

### 1. Introduction

Lake eutrophication caused by wastewater is widespread in the world. With the continuous increase of global population and the intensification of human activities, the global wastewater discharge is increasing (UN Environment Programme, 2023), and the degree of water eutrophication is also deepening. The survey report of the World Environment Situation Room points out that with the increase of the degree of eutrophication of water bodies, the frequency of bloom outbreak has increased globally (World Water Quality Alliance, 2021). When blooms occur, the water environment is rapidly damaged (Mandal et al., 2024). And has a profound negative impact (Jia et al., 2024) on social and economic development, so the treatment of polluted water bodies has been paid more and more attention. There are physical, chemical, and biological (Song et al. 2024) methods to control the blooms, among which the physical method can reduce the density of algae in a short time and rapidly improve the water quality as an important means (Liu et al., 2024) to deal with the blooms.

Flocculation-air floatation is one (Li et al., 2024a; Leite et al., 2019) of the most commonly used physical methods. The existing equipment is used to complete the flocculation-air floatation by mechanical stirring, and the removal efficiency of the flocculation-air floatation is improved by changing the formation mechanism (Al-Zoubi et al., 2015; Wang et al., 2023) of bubbles (Zhao et al., 2024; Xu et al., 2024), modifying bubbles, modifying particles (Liang et al., 2022; Wang et al., 2021) and optimizing flow field distribution (Wang et al., 2025). However, the scheme of mechanical stirring generating floc still has the problem (Nie et al., 2021) that it covers a large area and the flow field generated by stirring is difficult to control.

Aiming at the shortage of mechanical stirring scheme, a scheme of completing flocculation-air flotation by tubular flocculation reactor equipment was proposed. This equipment generates a specific flow field (Wang et al., 2023) by centrifugal force and wall effect of the tube wall, so as to achieve the purpose of collecting algae particles in the fluid and producing floc. Previous studies have found that the floc produced by the tube-based flocculation reactor floats faster and consumes less (Zhang et al., 2023) chemicals than the floc produced by mechanical agitation. This allows the reactor to occupy a smaller area than the mechanical stirring type, and because there are no moving parts in the pipeline, the flow field in the pipeline is much easier to control than the mechanical stirring type. However, the existing research have not clarified the influencing factors of the flow field changes in the reactor and the influencing mechanism of the flow field on the floc growth, which leads to the design and industrial application of the reactor are greatly limited.

In this study, the combination (Sepulveda et al., 2024) of simulation and experiment was used to compare the influence of different conditions on the shape of flocs and the difference of flocs generated by different flow fields. Specifically, computational fluid mechanics was used to simulate the distribution law (Oliveira et al., 2024) of flow field, and high-speed cameras were used to photograph the shapes (Tomin et al., 2023) of floc generated by Dianchi Lake bloom in a tubular flocculation reactor under different conditions. The experiment was a uniform experiment with corresponding experimental results for each simulation condition, and the flow field generated under different conditions and corresponding floc shapes were obtained by combining the experimental results with the simulation results. The influence mechanism of the initial conditions on the fluid and the flow field was explored, and the characteristics of the flow field and the shape of the floc were compared under different conditions, so as to explore how to generate the floc with different shapes.

## 2. Materials and methods

### 2.1. Subsection

#### 2.1.1. Lab equipment

As shown in Fig. 1, the tubular flocculation reactor is a continuous system consisting of a diaphragm pump with adjustable flow rate, two peristaltic pumps for dispensing poly aluminum chloride (PAC) and poly acrylamide (PAM) reagents, a spiral tube reactor and a filming device. The camera is a 200mm\*50mm\*10mm square container made of polymethyl methacrylate material, the bottom of the container has an inlet with an inner diameter of 10mm, the outlet of the spiral tube reactor is directly connected with the camera, and the top of the container is connected with the atmospheric side to set up an outlet with an inner diameter of 20mm. After supplementing the light for the device, a high-speed camera is used to photograph the floc at the outlet of the reactor and the results are stored in the computer. Three kinds of spiral tube reactors were made, with a radius of 100mm and a pipe spacing of 1mm. PVC pipes of 6mm, 12mm and 20mm were respectively used to surround the reactor. The parameters of equipment used are shown in Table 1.

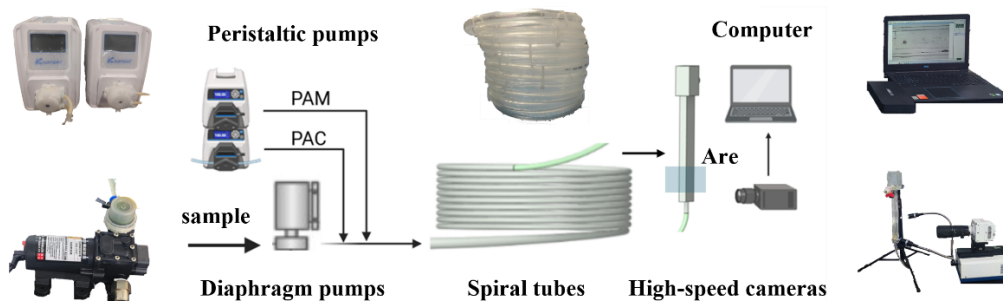


Fig. 1. Schematic diagram of tubular flocculation reactor experiment

#### 2.1.2 Lab equipment

The samples used in the experiment were collected from Dianchi Lake, and the sampling point coordinates were (102.6676559, 24.9020226). Located in Kunming, Yunnan Province, China, Dianchi

Lake is a typical plateau lake where seasonal blue-green algae blooms often occur. Light microscope analysis found that microcystis aeruginosa was the dominant species in the collected samples, and the concentration of algal cells in the samples was characterized by absorbance measured by a spectrophotometer at 680nm wavelength.

Table 1. Use of equipment and agents

Project	Specification
Diaphragm pumps	0.2-5 L min <sup>-1</sup>
Peristaltic pumps	0.1-0.7 mL s <sup>-1</sup>
Spectrophotometer	DR6000, HACH, USA
High-speed camera	EO-410 L, Phantom, USA
Spiral tubes length	6700 mm
Spiral tubes radius	100 mm
Spiral tubes inner diameter	6 12 20 mm
Bubble machine	GWNB1, Gongyuan, China

PAC and PAM were roasted in an oven at 60°C for 3 hours and then weighed 5g with an electronic balance and dissolved 5L of pure water to prepare two bottles of solution with a concentration of 1g·L<sup>-1</sup> for later use. The experimental steps are as follows:

- (1) The samples, reagents, and bubbly water were introduced into the inlet of the helical reactor at a constant rate. The samples and reagents were pumped in using peristaltic pumps, with the reagents being PAC and PAM. The flow rate of the bubbly water was controlled by adjusting the valve size.
- (2) Liquids were directly introduced into the helical reactor. After the reaction in the reactor, two 500 ml cups of solution were collected at the outlet using beakers. Immediately, a high - speed camera was used to film for 60 seconds at a frame rate of 400 fps. After the filming, the setup was left undisturbed.
- (3) 400ml liquid is taken from the end of the reactor and 100ml bubble is passed into the reactor. Stand the liquid through the bubble for 3 minutes and then use the pipette to absorb the liquid at the bottom to measure OD<sub>680</sub> and calculate the removal efficiency. The effect of the water through the bubble should be removed during the efficiency calculation. The removal efficiency calculation formula is as follows:

$$(D_0 - \frac{D_3(L_1+L_2)-D_2L_2}{L_1})/D_0 \quad (1)$$

where  $D_0$  is the initial absorbance and the absorbance of the bubbling water.  $D_2L_1$  is the amount of liquid received by the reactor,  $L_2$  is the number of bubbles entered, and  $D_3$  is the absorbance of the liquid absorbed by the pipette.

The experiment adopts uniform experiment. During the experiment, the sample concentration, the flow rate in the pipeline, the concentration of the agent, the inner diameter of the pipeline and the length of the pipeline need to be changed. The detailed parameters are shown in Table 2. The dosage of the drug is controlled by the pumping speed of the peristaltic pump and the flow rate of the fluid in the pipeline is controlled by the diaphragm pump.

Table 2. Experimental parameters

Item	parameter
Algae OD <sub>680</sub>	0.1, 0.2, 0.4, 0.6, 1.0
Concentration of PAC (mg·L <sup>-1</sup> )	3, 5, 20, 40, 60, 80, 100
Concentration of PAM (mg·L <sup>-1</sup> )	0.3, 0.5, 2, 4, 6, 8, 10
Velocity of sample (m s <sup>-1</sup> )	0.15, 0.2, 0.25, 0.3
Length of pipeline (m)	6.7, 6, 5.5, 5, 4.5, 4, 3.5, 3, 2.5, 2, 1.5, 1
Pipe diameter (mm)	6, 12, 20

### 2.1.3. Video processing

The video processing scheme is shown in Fig. 2. By analyzing the collected video, the size and fractal dimension of the floc in the video are obtained to determine whether the floc generated by the reactor is compact, as follows:

- (1) Length calibration: Before video shooting, adjust the lens focal length until the particles are clear and place a ruler with length in the shooting window. The software Imagej calculates the number of pixels corresponding to the ruler per unit length, and the corresponding relationship  $p$  between the length and pixels is obtained, and the result is  $20 \mu\text{m px}^{-1}$ .
- (2) Image framing: the video shot by the high-speed camera is stored in the format of cine, and the recognition program is written in python and OpenCV library for post-processing. The image is composed of  $1280 \times 800$  pixels, the corresponding shooting window is  $25\text{mm} \times 10\text{mm}$ , and the first 40000 frames of the video are processed. During the experiment, the slowest flow rate was  $0.1\text{m s}^{-1}$ . Every 100 frames of particles passed through a height of at least  $10\text{mm}$ . In order to avoid repeating the statistics of particles, the if function was used to determine whether the number of frames in the video could be evenly divided by 100 to extract the image frames to be processed.
- (3) Particle extraction: Sobel operator is used to identify particle boundaries after video image extraction. Sobel operator is an algorithm to identify particle edges in images by calculating the rate of change of gray value of gray image. The algorithm is realized through the following calculation.

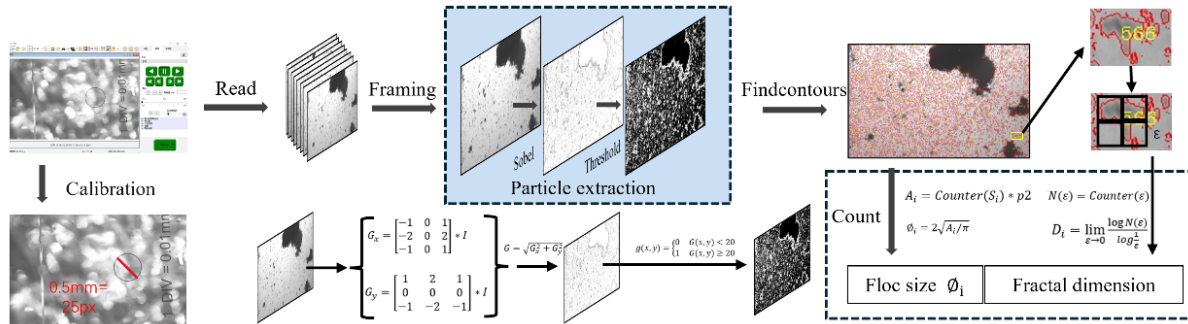


Fig. 2 Video processing scheme

$$G_x = \begin{bmatrix} -1 & 0 & 1 \\ -2 & 0 & 2 \\ -1 & 0 & 1 \end{bmatrix} * I, \quad G_y = \begin{bmatrix} 1 & 2 & 1 \\ 0 & 0 & 0 \\ -1 & -2 & -1 \end{bmatrix} * I, \quad (2)$$

$I$  is the video image, and the formula is used after processing the video image:

$$G_i = \begin{cases} G_i = |G_i| & -255 < G_i < 255 \\ G_i = 255 & G_i < -255, G_i > 255 \end{cases} \quad (3)$$

To convert  $G_x$  and  $G_y$ , the result after conversion is given by the formula:

$$G = \sqrt{G_x^2 + G_y^2}. \quad (4)$$

Synthesize as grayscale map.

In order to facilitate the parameter extraction of the particle, the edge and other parts of the particle are binarized by threshold segmentation. The threshold segmentation formula for the gray level map is as follows:

$$g(x, y) = \begin{cases} 0 & G(x, y) < 20 \\ 1 & G(x, y) \geq 20 \end{cases} \quad (5)$$

Use the gray level of 20 to binarize the picture.

- (4) Parameter calculation: using contour detection 1 Surround the closed area, the area is the granular image, the contour detection adopts OpenCV's Findontours function, the input three parameters of the function are set to the image after threshold segmentation, each contour line is independent, and only the outermost layer is counted.

Findontours function by traversing the binary gray map, will meet the given value of all the pixels once, from the first point to detect whether there is an adjacent point to the closure, and the statistics of each pixel included in an array. When all the pixels in the image with a given value are traversed, output an array S containing all the closed areas and corresponding pixel points, and the closed area corresponding to S each particle is  $S_i$  (Suzuki and Abe, 1985).

Each closed  $S_i$  area will be analyzed separately, the pixels contained in the closed area will be counted, and the corresponding area can be obtained through the corrected length correspondence using the formula:  $A_i$

$$\begin{cases} A_i = \text{Counter}(S_i) * p^2 \\ \phi_i = 2\sqrt{A_i}/\pi \end{cases} \quad (6)$$

Calculate the particle size, the formula is the size of the floc.  $\phi_i$  The fractal dimension is calculated using the following formula:

$$\begin{cases} N(\varepsilon) = \text{Counter}(\varepsilon) \\ D_i = \lim_{\varepsilon \rightarrow 0} \frac{\log N(\varepsilon)}{\log \frac{1}{\varepsilon}} \end{cases} \quad (7)$$

where  $D_i$  is the fractal dimension of particle  $i$ ,  $N(\varepsilon)$  is the number of squares needed to cover the particle area, and  $\varepsilon$  is the side length of the corresponding square. It is obtained by filling, starting from the left side of the closed area to fill the square until the filled square does not contain the closed area of the pixel stop and count.  $\varepsilon$  The iterative method is adopted to reach the solution approaching 0, the initial value is half of the particle size, the scaling coefficient is 0.8, and the scaling will be carried out ten times. Scale  $\varepsilon$  ten times, and conduct a linear fit on the parameters  $\log \frac{1}{\varepsilon}$  and  $\log N(\varepsilon)$  calculated after each scaling. The slope thus obtained is  $D_i$ .

## 2.2. Simulation Settings

In the experiment, the pipe is arranged in a spiral line, and the pipe is stacked counterclockwise around the center. The total stack is stacked around ten layers, and the structure of each layer is similar. The pipe wall structure in the pipe does not change with the length, and the fluid is only affected by gravity. It can be considered that the experimental pipeline layout has symmetry. Considering the simulation needs and equipment computing power, the simulated pipeline is finally selected to surround  $360^\circ$  (628mm).

The mesh was swept along the direction of the pipeline in prismatic mode. The boundary layer was set to 0.1mm per layer for a total of 10 layers, the prismatic length was set to 0.7mm, and the maximum element size of the prismatic section direction was set to 4 uniform values ranging from 0.25 to 1mm to verify the mesh independence.

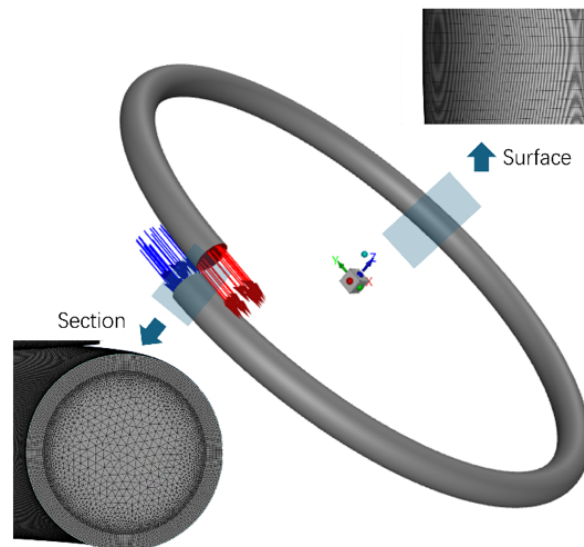


Fig. 3. Model and mesh setup

The final simulation model is shown in Fig. 3. The model is a 628mm long spiral tube with an encircling radius of 100mm and pipe spacing of 1mm. The inner diameter is set to 6mm, 12mm and 20mm, and the number of meshes is 70w, 80w, 90w and 100w according to the different cell scales. Since the simulation model is a spiral tube, the fluid in the pipe is affected by inertia, the force in the model is not uniform, and the direction of Reynolds pressure is inconsistent, so the RSM model is used to describe the fluid flow (Lauder et al., 1975). By analyzing the quality of the mesh, it can be found that more than 90% of the mesh scale falls near the 0.278 scale, the skew of the mesh is extremely low, the mesh is approximately a single scale distribution, and the mesh quality is high, which can meet the needs of Fluent solver.

Table 3. Mesh Settings

Mesh scale	Inflation	Y+	Element Quality	Max Aspect Ratio	Number of mesh
mm	mm				
0.25	1	0.1	0.225	9.9	1×10 <sup>6</sup>
0.5	1	0.1	0.278	6.04	9×10 <sup>5</sup>
0.75	1	0.1	0.199	5.63	8×10 <sup>5</sup>
1	1	0.1	0.187	5.59	7×10 <sup>5</sup>

Q criterion (Hunt et al., 1988) is used to evaluate the flow field distribution state in tubular flocculation reactor, where it is called rotation rate or vorticity tensor and is called strain rate tensor. Therefore, it can be concluded that when Q value is positive, the rotation rate or vorticity tensor is dominant, and when Q value is negative, the strain rate tensor is dominant. The simulation adopts single-phase flow simulation and uses standard wall model to deal with the fluid near the wall. The formulas involved in the simulation are shown in Table 4 below.

Table 4. Formulas involved in the simulation

Items	Models
Velocity	$u_i = \bar{u}_i + u_i'$
Continuity equation	$\frac{\partial}{\partial t}(\rho u_i) + \frac{\partial}{\partial x_j}(\rho u_i u_j)$ $= -\frac{\partial p}{\partial x_i} + \frac{\partial}{\partial x_j} \left[ \mu \left( \frac{\partial u_i}{\partial x_j} + \frac{\partial u_j}{\partial x_i} \right) \right] + \frac{\partial}{\partial x_j} (-\rho \bar{u}_i \bar{u}_j)$
Motion equation	$\frac{\partial}{\partial t}(\rho \bar{u}_i \bar{u}_j) + \frac{\partial}{\partial x_k}(\rho u_k \bar{u}_i \bar{u}_j)$ $= -\frac{\partial}{\partial x_k} \left[ \rho \bar{u}_i \bar{u}_j \bar{u}_k + p (\delta_{kj} \bar{u}_i + \delta_{jk} \bar{u}_i) \right]$ $- \rho \left( \bar{u}_i \bar{u}_k \frac{\partial u_j}{\partial x_k} + \bar{u}_j \bar{u}_k \frac{\partial u_i}{\partial x_k} \right)$ $+ \rho \left( \frac{\partial \bar{u}_i}{\partial x_j} + \frac{\partial \bar{u}_j}{\partial x_i} \right) - 2\mu \frac{\partial \bar{u}_i}{\partial x_k} \frac{\partial \bar{u}_j}{\partial x_k}$
Second Order Upwind	$\left( u \frac{\partial \phi}{\partial x} \right)_i = \frac{u_i}{2\Delta x} (3\phi_i - 4\phi_{i-1} + \phi_{i-2}), \quad u_i > 0$ $\left( u \frac{\partial \phi}{\partial x} \right)_i = \frac{u_i}{2\Delta x} (-3\phi_i + 4\phi_{i-1} - \phi_{i-2}), \quad u_i < 0$
Standard wall function	$\frac{U_p 0.09^{1/4} k_p^{1/2}}{\tau_w / \rho} = \frac{1}{0.4187} \ln(9.793 \frac{\rho 0.09^{1/4} k_p^{1/2} y_p}{\mu})$
Q criterion	$Q = 0.5 \left[ \left\  0.5 \left[ \frac{\partial u_i}{\partial x_j} - \frac{\partial u_j}{\partial x_i} \right] \right\ ^2 - \left\  0.5 \left[ \frac{\partial u}{\partial x_i} + \frac{\partial u}{\partial x_j} \right] \right\ ^2 \right]$ $\Omega = 0.5 \left[ \frac{\partial u_i}{\partial x_j} - \frac{\partial u_j}{\partial x_i} \right]$ $S = 0.5 \left[ \frac{\partial u}{\partial x_i} + \frac{\partial u}{\partial x_j} \right]$

The simulated inlet velocity of Tubular Coagulation Reactor is  $0.15\text{-}0.3\text{m s}^{-1}$  perpendicular to the inlet section, and the outlet pressure is set as 1 standard atmosphere. The solver set to simplec calculates the pressure and momentum using the Second Order Upwind and initializes the model using water. The simulation was carried out using fluent 2021R1. The software ran on the E5-2696 V3 processor, and 30 logical processors were used to calculate the simulation results for 60s to ensure that the flow field entered a stable state. The simulation time in each case was 200 hours.

### 3. Results and discussion

#### 3.1. Image recognition parameter determination and simulation independence verification

The above calculation methods of fractal dimension and floc size were used to make statistics on the floc flocculation process in the shooting area Are in FIG. 2. Fig. 4 shows the schematic diagram of the iterative residual changes of fractal dimensions of different floc sizes. 680 particles of the filmed video were scaled for 30 times, and the calculated results were divided into four intervals according to the floc size at an interval of  $100\mu\text{m}$  and averaged together with the whole. It can be found that the iterative residual decreases rapidly as the number of iterations increases. After 10 times of scaling, the iterative residual less than 0.01 and the proportion less than 0.1% can be ignored, and 10 times of scaling is adopted in the final calculation. The size of the floc is only related to the result of shooting, and the scaling of the picture does not affect the statistic floc size.

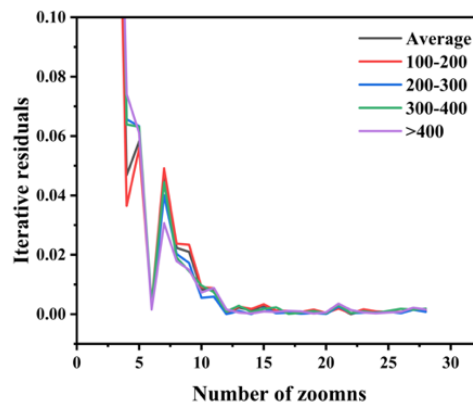


Fig. 4. Iterative residuals of fractal dimensions of different floc sizes

Before CFD simulation is carried out to study the flow field distribution in a Tubular Coagulation Reactor, it is necessary to verify the mesh to eliminate the calculation errors caused by unreasonable mesh Settings. As shown in Fig. 5, the 12mm pipe diameter model is taken as an example to simulate the model with different number of mesh, and the Q criterion parameters for calculation of different number of mesh are output. Fig. 5(A) shows the calculation results of different number of mesh along the pipe length direction Q, Fig. 5(B) is the calculation result diagram of different mesh numbers along the pipe diameter direction Q, legend 0mm is the center of the pipe, negative value is the inside. The simulation data shows that when the number of mesh is greater than  $9 \times 10^5$ , the calculation results of the Q criterion will no longer change with the increase of the number of mesh, and the final simulation adopts the model of 910 mesh.

#### 3.2. Study on the influence of floc shape on removal efficiency in Tubular Coagulation Reactor

Fig. 6 shows the study on the removal efficiency of wild algae by Tubular Coagulation Reactor with different pipe diameters at 0.2 algal cell concentration. As shown in Fig. 6(A), the removal efficiency of algae by tubular flocculators with diameters ranging from 6 to 20 mm can reach over 90% in natural water. With the increase of the combined dosage of PAC and PAM flocculants, the removal efficiency of the three kinds of tubular flocculants was significantly improved at first and then stabilized. When the dosage of the flocculant was doubled, the removal efficiency of algae in all three tube flocculants showed a downward trend. Zhang et al. (2023) observed a similar phenomenon (Zhang et al., 2023) in which algal removal efficiency initially increased but then significantly decreased with increasing

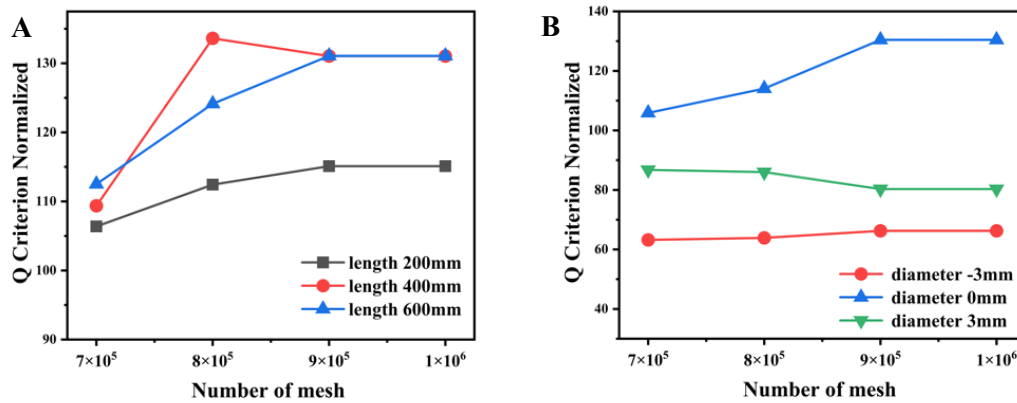


Fig. 5. Influence of the number of mesh on the calculation results (A. Q criterion parameter of tube length direction; B. Q criterion parameter of pipe diameter direction)

agent concentrations in a Tubular Coagulation Reactor. This phenomenon is not observed in conventional mechanical agitation flotation, and the amount of flocculant required for tubular flocculation is reduced by more than 50% compared to conventional mechanical agitation flocculation.

As the concentration of flocculant increased, the size of the flocs formed in all three tubular diameter reactors increased, as shown in Fig. 6(B): The flocs in the reactors with diameters of 12 and 20mm reached the maximum size of 850 $\mu\text{m}$  and 1000 $\mu\text{m}$ , respectively, when PAC and PAM concentrations were 40mg  $\cdot\text{L}^{-1}$  and 4mg  $\cdot\text{L}$ . The floc size decreased as the agent concentration continued to increase, and the experimental data showed that the maximum floc size also increased with the increase of tube diameter. This indicates that larger reactor diameter is conducive to the formation of larger floc size.

The statistics of the fractal dimension also showed that the morphology of the floc had a similar rule, as shown in Fig. 6(C): With the increase of the concentration of the reagent, the fractal dimension of the floc generated in the three reactors increased first and then decreased, and reached the maximum value when the concentration of PAC and PAM was 40mg  $\cdot\text{L}^{-1}$  and 4mg  $\cdot\text{L}$ . This indicates that there is an optimal value of the dosage of flocculant, near which the generated floc is large and compact, and excessive or insufficient agent will hinder the formation of floc, resulting in smaller and looser floc.

After determining the relationship between different pipe diameters and drug doses on floc and removal efficiency, it is not difficult to find that there is a certain relationship between floc morphology and removal efficiency. By drawing the bubble diagram as shown in Fig. 6(D), it can be found that the fractal dimension increases with the increase of floc particle size, while the removal efficiency increases rapidly, reaching the maximum value when the fractal dimension is 1.25 for the floc particle size of 900 $\mu\text{m}$ . At this time, the removal efficiency is above 90%. This indicates that the quality of the generated floc directly affects the removal efficiency, and the possible direction to increase the removal efficiency is to study how to generate higher quality floc in order to more efficiently separate algal cells from water.

As shown in Fig. 7, the changes of floc characteristics obtained after different initial concentrations of PAC and PAM were injected into the 12mm tubular reactor under the conditions of 60mg  $\cdot\text{L}^{-1}$  and 6mg  $\cdot\text{L}$ . It can be found that the size and fractal dimension of floc both increased with the increase of initial concentration and reached the limit when the concentration was increased to 0.4. This indicates that increasing the concentration of algal cells will have an impact on flocculation when the drug dose remains unchanged, and it is necessary to accurately control the dosage of flocculant combined with the sample concentration.

The Tubular Coagulation Reactor is a spiral tube structure. Due to the action of inertia, vortex is generated in the pipeline under the action of the pressure difference between inside and outside and the pressure difference in the vertical direction, which drives particles to collide and adhere to each other. In this process, the flocculant changes the surface charge of the particles to make the particles tend to be neutral so as to reduce the mutual repulsion between the particles and thus increase the probability of polymerization. With the change of the surface charge of the particles, the agent will cause the repulsion between the particles again, resulting in the decline of the flocculation efficiency and the formation of small and loose flocs (Moruzzi et al., 2024).

In mechanical agitation flocculation, a large number of agents are usually required to observe this phenomenon of reduced flocculation efficiency due to excessive flocculation, but it is very easy to happen in tubular flocculation. It has been proved (Zhang et al., 2023) that only the precise control of the dosage of flocculant can generate the required flocs shape to achieve efficient flocculation.

### 3.3. The driving mechanism of flow field on floc formation in Tubular Coagulation Reactor

The formation of floc is affected by the collision and adsorption of particles, and the removal efficiency of different shapes of pipes is completely different. Therefore, it is necessary to study the mechanism of flow field in the process of floc formation. As shown in Fig. 8, the shape characteristics of the floc generated in the Tubular Coagulation Reactor of different lengths and the simulation results of corresponding specifications are presented. The simulation results use Q criterion to characterize the

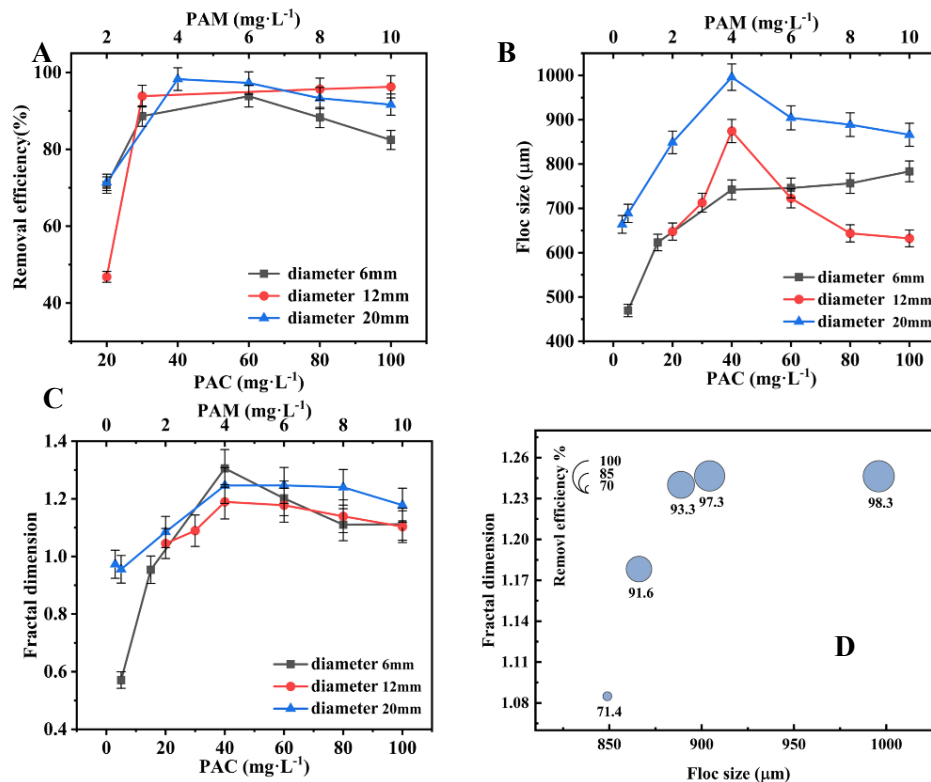


Fig. 6. Effects of pipe diameter and drug dose on floc shape and removal efficiency (A. Removal efficiency is affected by pipe diameter and drug concentration; B. Floc size was affected by tube diameter and reagent concentration; C. Fractal dimension was affected by pipe diameter and reagent concentration; D. Effects of floc size and fractal dimension on removal efficiency)

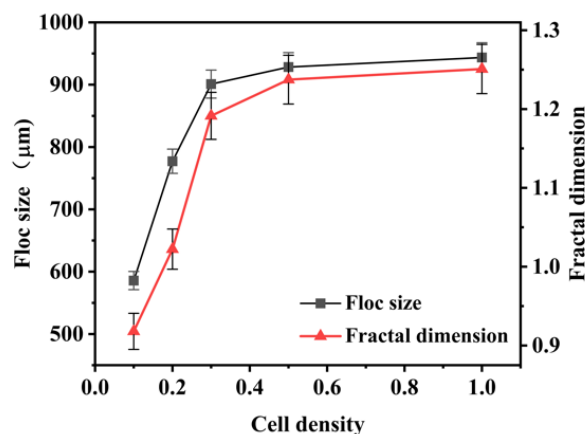


Fig. 7. Effect of initial algal concentration on floc

flow field distribution in the flow field. As the pipe length increases from 0.5m to 6.7m, as shown in Fig. 8(A), the fractal dimension and floc size of the generated floc increase uniformly. Simulation data 8(B) shows the variation trend of Q criterion in the direction of pipe length at different positions. The spiral pipe is measured as a negative value with zero as the center point, and the drastic change of flow field in the pipeline only occurs within 200mm distance from the entrance, and the flow field tends to be stable with the increase of distance. Comprehensive experimental and simulation results show that after the fluid enters the pipeline 200mm, the flow field becomes stable. The flow field in the pipeline is uniform and stable without drastic changes, and the factor affecting the production of floc is stability.

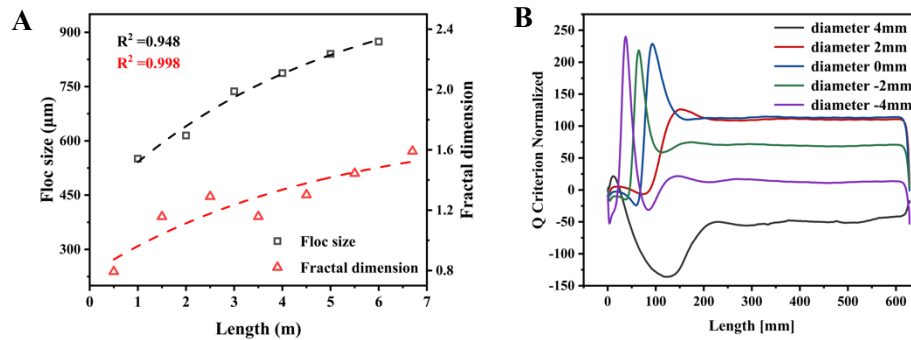


Fig. 8. Distribution of Q criteria and floc shape in different tubes (A. Change of floc shape with tube length; B. Q criterion distribution along pipe length direction at different positions in pipe diameter direction)

Affected by this factor, flocs roll with the water flow in the pipe and wrap more unstable cells or clusters, resulting in a more compact structure. Therefore, large flocs with sufficient compactness require reactors at sufficient distances to provide sufficient aggregation time, while too long reaction time will cause the flocs to be destroyed by excessive hydraulic shear.

In order to determine the factors affecting the flow field on the floc formation, it is necessary to analyze the changes of the flow field generated by different reactors and different working conditions.

Fig. 9 shows the flow field generated by the Tubular Coagulation Reactor under the condition of a flow rate of  $0.2\text{m s}^{-1}$  with different pipe diameters of 318mm tubes and the floc morphology generated by the reactor of corresponding specifications. Fig. 9(A) shows the flow field distribution in the pipeline under different pipe diameters. The left side is the inner part of the spiral pipe, and the right side is the outer part. The diagram shows that the strength of the vortex increases at the two walls near the inner part of the pipeline, while the strength of the vortex decreases at the wall near the outer part. This is because the pipe is arranged in a spiral way, and the flow velocity on the outside is higher than that on the inside under the action of inertial force, resulting in the fluid distribution in the pipe showing the illustrated structure. As the diameter of the pipe increases, the proportion of the area where the flow velocity increases decreases, and the influence of the flow velocity difference on the whole decreases.

Fig. 9(B) shows the proportion of areas with non-positive Q in models with different pipe diameters. It can be found that the proportion of non-positive areas in the 6mm pipe is larger than that in the 20mm pipe, and the proportion of non-positive areas in the 6mm pipe is the smallest. The reason for this change is not clear, and existing studies can only show that this phenomenon may be related (Bassinov et al., 2024) to the viscous force of the fluid. The distribution law of the region where Q is not positive in the pipeline is consistent with the change law of the size and fractal dimension of the floc measured by different pipe diameters in Fig. 9(C) under the condition of flow rate of  $0.2\text{m s}^{-1}$ .

The research shows that the area where the flow field has a great influence on particle motion is the inertial subregion of the turbulent energy spectrum, which corresponds to the region where the vortices change from large to small. In this region, the large vortices break into several smaller vortices. In the process of vortex breaking, the energy loss causes the flow lines to be close to each other, and the particles carried in the flow site are also close to each other, resulting in the agglomeration and flocculation of particles (Li et al., 2024b). The determination of this region coincides with the definition of the Q criterion, where the vortex rotation rate of the inertia subregion decreases,  $\Omega$  decreases, and S begins to dominate, corresponding to the non-positive region of the Q criterion. The distribution law of Q value can reflect the distribution of inertia sub-interval to a certain extent.

The influence of flow rate on floc generation is shown in Fig. 10, in which Fig. 10(A) is the distribution cloud of Q criterion in pipelines with different flow rates. As the speed increases, it can be seen that the position of Q criterion region does not change, and the maximum value increases (Zhou et al., 2025), while the distribution of non-positive region of Q criterion decreases with the increase of flow rate, as shown in Fig. 10(B). The proportion of the inertia subinterval represented by the non-positive region of the Q criterion also decreases (Wang et al., 2025), which leads to the simultaneous decline of the size and fractal dimension of the generated floc in the actual experiment shown in Fig. 10(C).

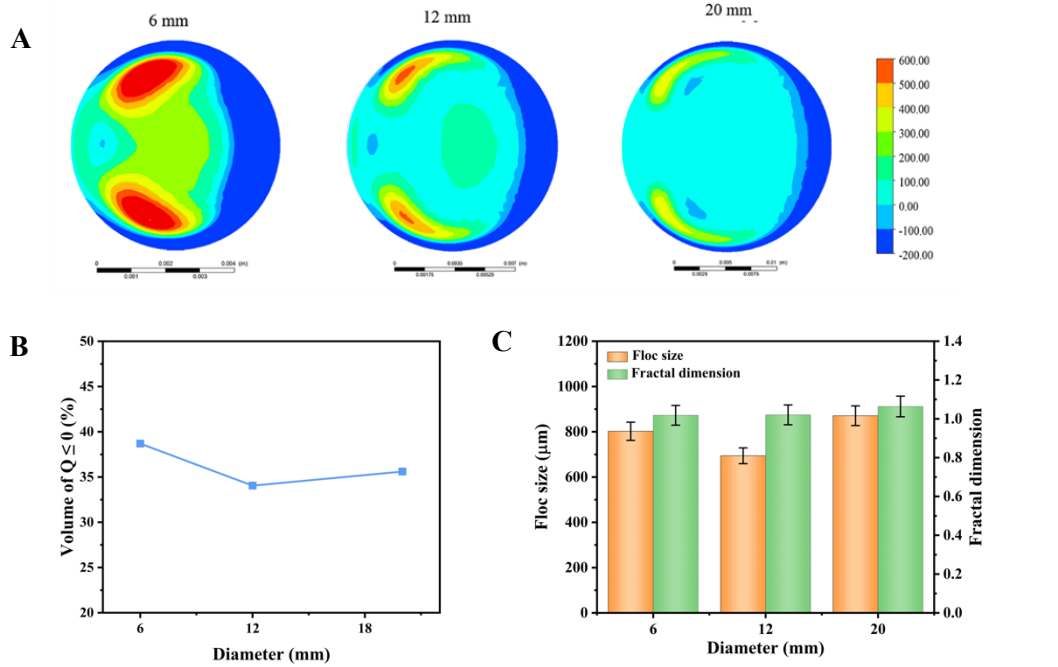


Fig. 9. Differences of floc formation in different pipe diameters (A. Distribution cloud map of Q criterion of 314mm pipe diameters; B. Ratio of non-positive area to flow field according to Q criterion of different pipe diameters; C. Size and fractal dimension of flocs generated by different pipe diameters)

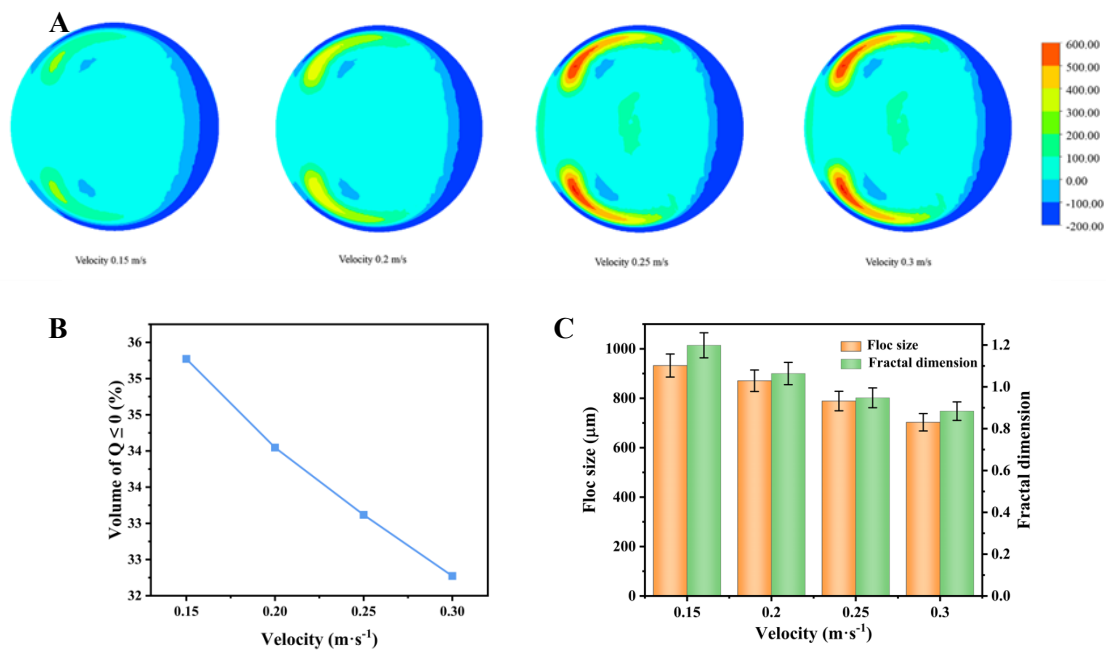


Fig. 10. Differences of floc formation at different flow rates (A. Distribution of Q criteria for 314mm tubes at different flow rates; B. The ratio of the non-positive area to the flow field according to the Q criterion at different flow rates; C. Floc size and fractal dimension generated at different flow rates)

Considering the proportion of inertia subinterval and the morphological characteristics of floc, as shown in Fig. 11, it is the comparison result of floc size and fractal dimension with the non-positive region of Q criterion. Fig. 11(A) is the fitting result of 6mm pipeline, and Fig. 11(B) is the fitting result of 12mm pipeline. The fitting results show that the size and fractal dimension of the generated floc of different pipe diameters are linearly correlated with the proportion of the non-positive region of the Q criterion, and the size and compactness of the generated floc of the pipe increase with the increase of the proportion region (Li et al., 2025).

Therefore, a hypothesis was proposed that the flow field distribution in the Tubular Coagulation Reactor could be changed by adjusting the pipe diameter and flow velocity. Changes in the flow field distribution would lead to changes in the proportion of inertial sub-intervals in the reactor, which would lead to a decrease in the contact probability of particles in the fluid and eventually be reflected in the change of floc morphology (Sun et al., 2025). Increasing the proportion of the inertia subinterval can increase the size and compactness of the floc, which has a positive impact on the separation.

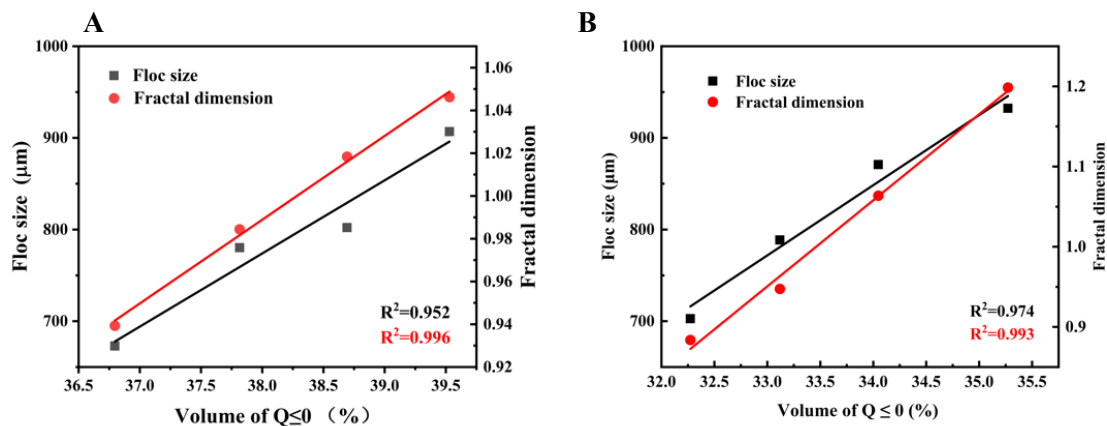


Fig. 11. Relationship between the distribution of Q criterion and the shape of floc (A. Distribution relationship between the shape of 6mm pipe floc and the Q criterion; B. Distribution of 12mm floc shape and Q criterion)

#### 4. Conclusions

Based on the Tubular Coagulation Reactor, combined with experiments and CFD simulation, this study deeply discussed the effects of flow field distribution, reagent concentration and algae concentration on the removal efficiency of tubular flocculation reactor, proposed parameters to characterize the flow field state, and established the correlation between them and the shape of flocs generated. The conclusions are as follows:

- (1) The removal efficiency of the tubular flocculation reactor is related to the particle size and fractal dimension of the generated flocs. The larger the flocs and the higher the fractal dimension, the higher the removal efficiency. When the floc size exceeds  $900 \mu\text{m}$  and the fractal dimension is greater than 1.25, the removal efficiency of the tubular coagulation reactor exceeds 90%. As the size and compactness of the generated flocs continue to increase, the removal efficiency will slowly rise, but the increase is minimal. Ultimately, the removal efficiency can reach over 98%.
- (2) The formation of the optimal floc shape requires precise regulation of the flow field, the concentration of the agent and the treated sample. Q criterion can be used to characterize the flow field distribution in the reactor. When the concentration of the sample is 0.2, the optimal dosage of PAC and PAM are  $40\text{mg} \cdot \text{L}^{-1}$  and  $4\text{mg} \cdot \text{L}^{-1}$ . The change of algal concentration will lead to the change of the optimal agent point, and the increase of algal concentration requires the simultaneous increase of the dosage of the agent.
- (3) The proportion of non-positive region of Q criterion can represent the proportion of inertia subinterval in the flow field, and the size and compactness of the generated floc are linearly correlated with the proportion of non-positive region of Q criterion. After the flow rate is increased from  $0.15\text{m} \cdot \text{s}^{-1}$  to  $0.3\text{m} \cdot \text{s}^{-1}$ , the non-positive region of Q criterion in the pipeline is reduced by 3%, the size of floc is reduced by  $200\mu\text{m}$ , and the fractal dimension is decreased by 0.3.

## Acknowledgments

The University Synergy Innovation Program of Anhui Province (GXXT-2023-104); Anhui Province Coal Clean Processing and Carbon Reduction Engineering Research Center Foundation (CCCE-2023001); China Postdoctoral Science Foundation (2020M671837); Anhui postdoctoral Foundation (2021A479).

## References

- AL-ZOUBI, H., IBRAHIM, K.A., ABU-SBEIH, K.A., 2015. *Removal of heavy metals from wastewater by economical polymeric collectors using dissolved air flotation process*, Journal of Water Process Engineering, 8, 19-27.
- BOSSINOV, D., RAMAZANOVA, G., TURALINA, D., 2024. *Comparison of measured and calculated high-viscosity crude oil temperature values in a pipeline during continuous pumping and shutdown modes*, International Journal of Thermofluids, Volume 24, 00950.
- HUNT, J.C., WRAY, A.A., MOIN, P., 1988. *Eddies stream and convergence zones in turbulent flows*. Cent. Turbul. Res. CTR-S 88, 193-208.
- JIA R., YANG Z., XIA R., et al. 2024. *Water pollution control promotes sustainable water use in Yangtze River Economic Belt – from water footprint perspective*. Environment, Development and Sustainability, 1-21.
- LAUNDER, B., REECE, G.J., RODI, W., 1975. *Progress in the development of a Reynolds-stress turbulence closure*. Journal of fluid mechanics 68, 537-566
- LEITE L.S., HOFFMANN, M.T., DANIEL, L.A., 2019. *Coagulation, and dissolved air flotation as a harvesting method for microalgae cultivated in wastewater*, Journal of Water Process Engineering, 32, 100947.
- LI, X., SUN, Z., WANG, H., WANG, L., YAN, X., ZHANG, H., RAN, J., LIU, J., 2025. *Particle motion under turbulent eddies: Inspiration for fine minerals flotation*, Chemical Engineering Science, 301, 120754.
- LI, X., SUN, Z., WANG, H., WANG, L., YAN, X., ZHANG, H., RAN, J., LIU, J., 2025. *Particle motion under turbulent eddies: Inspiration for fine minerals flotation*, Chemical Engineering Science, Volume 301, 120754.
- LI, P., ZHANG, J., SHEN, Y., FENG, X., JIA, W., LIU, M., ZHAO, S., 2024. *Efficient, quick, and low-carbon removal mechanism of microplastics based on integrated gel coagulation-spontaneous flotation process*, Water Research, Volume 259, 121906.
- LIANG, L., LUO, J., XIAO, X., WANG, J., HONG, M., DENG, C., LI, Y.-Y., LIU, J., 2022. *Granular activated carbon promoting re-granulation of anammox-hydroxyapatite granules for stable nitrogen removal at low phosphate concentration*, Science of The Total Environment, 805, 15035.
- LIU M, WU J, LIANG J, et al. 2024. *Cyanobacterial blooms management: A simulation-based optimization method*. Journal of environmental management, 370 122639
- MANDAL A., BISWAS S., TIWARI K.P., et al. 2024. *Seasonal refuge patterns of phytoplankton trigger irregular bloom events in a contaminated environment*. Scientific Reports, 14(1), 25248-25248.
- MORUZZI, R.B., DE OLIVEIRA, A.R., SHARIFI, S., BANKOLE, A.O., CAMPOS, R.C., 2024. *Enhancing flocculation kinetics assessment: Integrating aggregate size distribution into experimental and modelling frameworks*, Journal of Water Process Engineering, 63, 105433.
- NIE, C., HU, K., REN, W., ZHOU, P., DUAN, X., XIAO, L., WANG, S., 2021 2025. *Mechanical agitation accelerated ultrasonication for wastewater treatment: Sustainable production of hydroxyl radicals*, Water Research, 198, 117124.
- OLIVEIRA, J.P.S., MEDRONHO, R.A., SANTOS, F.P., KLEIN, T.S., 2025. *CFD multiphase modeling of liquid-liquid hydrocyclones: A review*, Journal of Industrial and Engineering Chemistry, 145, 33-62.
- SEPULVEDA, F.D., CORTES, L.A., ARANCIBIA-BRAVO, M.P., DELGADO, J., LUCAY, F.A., CHACANA, C., FELIPE GALLEGUILLOS, F., CASTELLON, C., 2024. *Optimizing flotation circuits: A comprehensive approach using design experiments and stochastic simulation in cycle test validation*, Minerals Engineering, 219, 108978.
- SONG Q.-X., HE, J., ZHU, H.-L., ZHENG, Z., HE, J., 2024. *An efficient polyaluminum lanthanum silicate coagulant for phosphorus removal and algal bloom control*, Journal of Environmental Chemical Engineering, 12(6), 114492.
- SUN, Z, LI, X., ZHAO, S., ZHONG, T., WANG, L., YAN, X., ZHANG, H., 2025. *Enhanced selective recovery of fine minerals in flotation by the oscillatory turbulence*, Journal of Environmental Chemical Engineering, 13(1), 115164.
- SUZUKI, S., ABE, K., 1985, *Topological Structural Analysis of Digitized Binary Images by Border Following*. CVGIP 30 1, 32-46.
- TOMIN, M., TOROK, D., PASZTHY, T., KMETTY, A., 2023. *Deformation analysis in impact testing of functionally graded foams by the image processing of high-speed camera recordings*, Polymer Testing, 122, 108014.
- UNITED NATIONS ENVIRONMENT PROGRAMME, 2023. *Wastewater - Turning Problem to Solution*. A UNEP Rapid Response Assessment. Nairobi. DOI: <https://doi.org/10.59117/20.500.11822/43142>

- WANG, B., CHEN, W., HUANG, J., LUO, S., GUO, C., YAN, X., ZHANG, H., WANG, L., *A modified model based on CFD simulation and experiments of chalcopyrite flotation*, Separation and Purification Technology, 355, 129634.
- WANG, C., LU, Y., YE, T., CHEN, L., HE, L., 2023. *Investigation on the mechanism of air/condensate bubble flotation of emulsified oil droplet*, Process Safety and Environmental Protection, 180, 554-565.
- WANG, H., CHEN, R., LI, D., ZHANG, B., YAN, X., RAN, J., ZHANG, H., 2025. *Probing the adaptability relationship between flow characteristics and mineral particles with different size and surface hydrophobicity*, Powder Technology, 452, 120588.
- WANG, L., CHENG, L., YIN, S., YAN, Z., ZHANG, X., 2023. *Multiphase slurry flow regimes and its pipeline transportation of underground backfill in metal mine: Mini review*, Construction and Building Materials, 402, 133014.
- WANG, Y., SUN, W., DING, L., LIU, W., TIAN, L., ZHAO, Y., ZHANG, M., WANG, X., 2021. *A study on the feasibility and mechanism of enhanced co-coagulation dissolved air flotation with chitosan-modified microbubbles*, Journal of Water Process Engineering, Volume 40, 101847.
- WORLD WATER QUALITY ALLIANCE, 2021. *World Water Quality Assessment: First Global Display of a Water Quality Baseline. A consortium effort by the World Water Quality Alliance - towards a full global assessment. Information Document Annex for display at the 5th Session of the United Nations Environment Assembly, Nairobi 2021.*
- XU, J., ZHANG, Y., WEN, K., WANG, X., YANG, Z., HUANG, Y., ZHENG, G., HUANG, L., ZHANG, J., 2024. *Enhanced removal of polystyrene nanoplastics by air flotation modified by dodecyltrimethylammonium chloride: Performance and mechanism*, Chinese Chemical Letters, 110240.
- ZHANG, H., LI, L., CHENG, S., LI, C., LIU, F., WANG, P., SUN, L., HUANG, J., ZHANG, W., ZHANG, X., 2023. *Enhanced Microcystis Aeruginosa removal and novel flocculation mechanisms using a novel continuous co-coagulation flotation (CCF)*, Science of The Total Environment, 857, 159532.
- ZHAO, Z., HUANG, X., ZHANG, Z., PANG, H., WANG, X., LI, P., LI, C., LU, J., 2024. *Removal efficiency and mechanism of geosmin by modified micro-nano bubbles in drinking water treatment process*, Journal of Water Process Engineering, Volume 60, 105125.
- ZHOU, R., LI, X., LI, D., WANG, H., SONG, Z., YAN, X., ZHANG, H., 2025. *The effect of energy input on bubble-particle collision, attachment, detachment, and collection efficiencies in a mechanical flotation cell*, Powder Technology, 453, 120659.